P H Y S I C A L   R E V I E W   L E T T E R S

Precision Measurement of the Ratio $\mathcal{B}(t \to Wb)/\mathcal{B}(t \to Wq)$ and Extraction of V_{tb}

V. M. Abazov,[35] B. Abbott,[73] B. S. Acharya,[29] M. Adams,[49] T. Adams,[47] G. D. Alexeev,[35] G. Alkhazov,[39] A. Alton,[61,†]
G. Alverson,[60] G. A. Alves,[2] M. Aoki,[48] M. Arov,[58] A. Askew,[47] B. Åsman,[41] O. Atramentov,[65] C. Avila,[8]
J. BackusMayes,[80] F. Badaud,[13] L. Bagby,[48] B. Baldin,[48] D. V. Bandurin,[47] S. Banerjee,[29] E. Barberis,[60] P. Baringer,[56]
J. Barreto,[3] J. F. Bartlett,[48] U. Bassler,[18] V. Bazterra,[49] S. Beale,[6] A. Bean,[56] M. Begalli,[3] M. Begel,[71]
C. Belanger-Champagne,[41] L. Bellantoni,[48] S. B. Beri,[27] G. Bernardi,[17] R. Bernhard,[22] I. Bertram,[42] M. Besançon,[18]
R. Beuselinck,[43] V. A. Bezzubov,[38] P. C. Bhat,[48] V. Bhatnagar,[27] G. Blazey,[50] S. Blessing,[47] K. Bloom,[64] A. Boehnlein,[48]
D. Boline,[70] E. E. Boos,[37] G. Borissov,[42] T. Bose,[59] A. Brandt,[76] O. Brandt,[23] R. Brock,[62] G. Brooijmans,[68] A. Bross,[48]
D. Brown,[17] J. Brown,[17] X. B. Bu,[48] M. Buehler,[79] V. Buescher,[24] V. Bunichev,[37] S. Burdin,[42,‡] T. H. Burnett,[80]
C. P. Buszello,[41] B. Calpas,[15] E. Camacho-Pérez,[32] M. A. Carrasco-Lizarraga,[56] B. C. K. Casey,[48] H. Castilla-Valdez,[32]
S. Chakrabarti,[70] D. Chakraborty,[50] K. M. Chan,[54] A. Chandra,[78] G. Chen,[56] S. Chevalier-Théry,[18] D. K. Cho,[75]
S. W. Cho,[31] S. Choi,[31] B. Choudhary,[28] S. Cihangir,[48] D. Claes,[64] J. Clutter,[56] M. Cooke,[48] W. E. Cooper,[48]
M. Corcoran,[78] F. Couderc,[18] M.-C. Cousinou,[15] A. Croc,[18] D. Cutts,[75] A. Das,[45] G. Davies,[43] K. De,[76] S. J. de Jong,[34]
E. De La Cruz-Burelo,[32] F. Déliot,[18] M. Demarteau,[48] R. Demina,[69] D. Denisov,[48] S. P. Denisov,[38] S. Desai,[48] C. Deterre,[18]
K. DeVaughan,[64] H. T. Diehl,[48] M. Diesburg,[48] P. F. Ding,[44] A. Dominguez,[64] T. Dorland,[80] A. Dubey,[28] L. V. Dudko,[37]
D. Duggan,[65] A. Duperrin,[15] S. Dutt,[27] A. Dyshkant,[50] M. Eads,[64] D. Edmunds,[62] J. Ellison,[46] V. D. Elvira,[48] Y. Enari,[17]
H. Evans,[52] A. Evdokimov,[71] V. N. Evdokimov,[38] G. Facini,[60] T. Ferbel,[69] F. Fiedler,[24] F. Filthaut,[34] W. Fisher,[62]
H. E. Fisk,[48] M. Fortner,[50] H. Fox,[42] S. Fuess,[48] A. Garcia-Bellido,[69] V. Gavrilov,[36] P. Gay,[13] W. Geng,[15,62] D. Gerbaudo,[66]
C. E. Gerber,[49] Y. Gershtein,[65] G. Ginther,[48,69] G. Golovanov,[35] A. Goussiou,[80] P. D. Grannis,[70] S. Greder,[19] H. Greenlee,[48]
Z. D. Greenwood,[58] E. M. Gregores,[4] G. Grenier,[20] Ph. Gris,[13] J.-F. Grivaz,[16] A. Grohsjean,[18] S. Grünendahl,[48]
M. W. Grünewald,[30] T. Guillemin,[16] F. Guo,[70] G. Gutierrez,[48] P. Gutierrez,[73] A. Haas,[68,§] S. Hagopian,[47] J. Haley,[60]
L. Han,[7] K. Harder,[44] A. Harel,[69] J. M. Hauptman,[55] J. Hays,[43] T. Head,[44] T. Hebbeker,[21] D. Hedin,[50] H. Hegab,[74]
A. P. Heinson,[46] U. Heintz,[75] C. Hensel,[23] I. Heredia-De La Cruz,[32] K. Herner,[61] G. Hesketh,[44,||] M. D. Hildreth,[54]
R. Hirosky,[79] T. Hoang,[47] J. D. Hobbs,[70] B. Hoeneisen,[12] M. Hohlfeld,[24] Z. Hubacek,[10,18] N. Huske,[17] V. Hynek,[10]
I. Iashvili,[67] Y. Ilchenko,[77] R. Illingworth,[48] A. S. Ito,[48] S. Jabeen,[75] M. Jaffré,[16] D. Jamin,[15] A. Jayasinghe,[73] R. Jesik,[43]
K. Johns,[45] M. Johnson,[48] D. Johnston,[64] A. Jonckheere,[48] P. Jonsson,[43] J. Joshi,[27] A. W. Jung,[48] A. Juste,[40] K. Kaadze,[57]
E. Kajfasz,[15] D. Karmanov,[37] P. A. Kasper,[48] I. Katsanos,[64] R. Kehoe,[77] S. Kermiche,[15] N. Khalatyan,[48] A. Khanov,[74]
A. Kharchilava,[67] Y. N. Kharzheev,[35] M. H. Kirby,[51] J. M. Kohli,[27] A. V. Kozelov,[38] J. Kraus,[62] S. Kulikov,[38] A. Kumar,[67]
A. Kupco,[11] T. Kurča,[20] V. A. Kuzmin,[37] J. Kvita,[9] S. Lammers,[52] G. Landsberg,[75] P. Lebrun,[20] H. S. Lee,[31] S. W. Lee,[55]
W. M. Lee,[48] J. Lellouch,[17] L. Li,[46] Q. Z. Li,[48] S. M. Lietti,[5] J. K. Lim,[31] D. Lincoln,[48] J. Linnemann,[62] V. V. Lipaev,[38]
R. Lipton,[48] Y. Liu,[7] Z. Liu,[6] A. Lobodenko,[39] M. Lokajicek,[11] R. Lopes de Sa,[70] H. J. Lubatti,[80] R. Luna-Garcia,[32,¶]
A. L. Lyon,[48] A. K. A. Maciel,[2] D. Mackin,[78] R. Madar,[18] R. Magaña-Villalba,[32] S. Malik,[64] V. L. Malyshev,[35]
Y. Maravin,[57] J. Martínez-Ortega,[32] R. McCarthy,[70] C. L. McGivern,[56] M. M. Meijer,[34] A. Melnitchouk,[63] D. Menezes,[50]
P. G. Mercadante,[4] M. Merkin,[37] A. Meyer,[21] J. Meyer,[23] F. Miconi,[19] N. K. Mondal,[29] G. S. Muanza,[15] M. Mulhearn,[79]
E. Nagy,[15] M. Naimuddin,[28] M. Narain,[75] R. Nayyar,[28] H. A. Neal,[61] J. P. Negret,[8] P. Neustroev,[39] S. F. Novaes,[5]
T. Nunnemann,[25] G. Obrant,[39,*] J. Orduna,[78] N. Osman,[15] J. Osta,[54] G. J. Otero y Garzón,[1] M. Padilla,[46] A. Pal,[76]
N. Parashar,[53] V. Parihar,[75] S. K. Park,[31] J. Parsons,[68] R. Partridge,[75,§] N. Parua,[52] A. Patwa,[71] B. Penning,[48] M. Perfilov,[37]
K. Peters,[44] Y. Peters,[44] K. Petridis,[44] G. Petrillo,[69] P. Pétroff,[16] R. Piegaia,[1] M.-A. Pleier,[71] P. L. M. Podesta-Lerma,[32,**]
V. M. Podstavkov,[48] P. Polozov,[36] A. V. Popov,[38] M. Prewitt,[78] D. Price,[52] N. Prokopenko,[38] S. Protopopescu,[71] J. Qian,[61]
A. Quadt,[23] B. Quinn,[63] M. S. Rangel,[2] K. Ranjan,[28] P. N. Ratoff,[42] I. Razumov,[38] P. Renkel,[77] M. Rijssenbeek,[70]
I. Ripp-Baudot,[19] F. Rizatdinova,[74] M. Rominsky,[48] A. Ross,[42] C. Royon,[18] P. Rubinov,[48] R. Ruchti,[54] G. Safronov,[36]
G. Sajot,[14] P. Salcido,[50] A. Sánchez-Hernández,[32] M. P. Sanders,[25] B. Sanghi,[48] A. S. Santos,[5] G. Savage,[48] L. Sawyer,[58]
T. Scanlon,[43] R. D. Schamberger,[70] Y. Scheglov,[39] H. Schellman,[51] T. Schliephake,[26] S. Schlobohm,[80]
C. Schwanenberger,[44] R. Schwienhorst,[62] J. Sekaric,[56] H. Severini,[73] E. Shabalina,[23] V. Shary,[18] A. A. Shchukin,[38]
R. K. Shivpuri,[28] V. Simak,[10] V. Sirotenko,[48] P. Skubic,[73] P. Slattery,[69] D. Smirnov,[54] K. J. Smith,[67] G. R. Snow,[64]
J. Snow,[72] S. Snyder,[71] S. Söldner-Rembold,[44] L. Sonnenschein,[21] K. Soustruznik,[9] J. Stark,[14] V. Stolin,[36]
D. A. Stoyanova,[38] M. Strauss,[73] D. Strom,[49] L. Stutte,[48] L. Suter,[44] P. Svoisky,[73] M. Takahashi,[44] A. Tanasijczuk,[1]
W. Taylor,[6] M. Titov,[18] V. V. Tokmenin,[35] Y.-T. Tsai,[69] D. Tsybychev,[70] B. Tuchming,[18] C. Tully,[66] L. Uvarov,[39]
S. Uvarov,[39] S. Uzunyan,[50] R. Van Kooten,[52] W. M. van Leeuwen,[33] N. Varelas,[49] E. W. Varnes,[45] I. A. Vasilyev,[38]

P. Verdier,[20] L. S. Vertogradov,[35] M. Verzocchi,[48] M. Vesterinen,[44] D. Vilanova,[18] P. Vokac,[10] H. D. Wahl,[47]
M. H. L. S. Wang,[48] J. Warchol,[54] G. Watts,[80] M. Wayne,[54] M. Weber,[48,††] L. Welty-Rieger,[51] A. White,[76] D. Wicke,[26]
M. R. J. Williams,[42] G. W. Wilson,[56] M. Wobisch,[58] D. R. Wood,[60] T. R. Wyatt,[44] Y. Xie,[48] C. Xu,[61] S. Yacoob,[51]
R. Yamada,[48] W.-C. Yang,[44] T. Yasuda,[48] Y. A. Yatsunenko,[35] Z. Ye,[48] H. Yin,[48] K. Yip,[71] S. W. Youn,[48] J. Yu,[76]
S. Zelitch,[79] T. Zhao,[80] B. Zhou,[61] J. Zhu,[61] M. Zielinski,[69] D. Zieminska,[52] and L. Zivkovic[75]

(D0 Collaboration)

[1]*Universidad de Buenos Aires, Buenos Aires, Argentina*
[2]*LAFEX, Centro Brasileiro de Pesquisas Físicas, Rio de Janeiro, Brazil*
[3]*Universidade do Estado do Rio de Janeiro, Rio de Janeiro, Brazil*
[4]*Universidade Federal do ABC, Santo André, Brazil*
[5]*Instituto de Física Teórica, Universidade Estadual Paulista, São Paulo, Brazil*
[6]*Simon Fraser University, Vancouver, British Columbia, and York University, Toronto, Ontario, Canada*
[7]*University of Science and Technology of China, Hefei, People's Republic of China*
[8]*Universidad de los Andes, Bogotá, Colombia*
[9]*Charles University, Faculty of Mathematics and Physics, Center for Particle Physics, Prague, Czech Republic*
[10]*Czech Technical University in Prague, Prague, Czech Republic*
[11]*Center for Particle Physics, Institute of Physics, Academy of Sciences of the Czech Republic, Prague, Czech Republic*
[12]*Universidad San Francisco de Quito, Quito, Ecuador*
[13]*LPC, Université Blaise Pascal, CNRS/IN2P3, Clermont, France*
[14]*LPSC, Université Joseph Fourier Grenoble 1, CNRS/IN2P3, Institut National Polytechnique de Grenoble, Grenoble, France*
[15]*CPPM, Aix-Marseille Université, CNRS/IN2P3, Marseille, France*
[16]*LAL, Université Paris-Sud, CNRS/IN2P3, Orsay, France*
[17]*LPNHE, Universités Paris VI and VII, CNRS/IN2P3, Paris, France*
[18]*CEA, Irfu, SPP, Saclay, France*
[19]*IPHC, Université de Strasbourg, CNRS/IN2P3, Strasbourg, France*
[20]*IPNL, Université Lyon 1, CNRS/IN2P3, Villeurbanne, France and Université de Lyon, Lyon, France*
[21]*III. Physikalisches Institut A, RWTH Aachen University, Aachen, Germany*
[22]*Physikalisches Institut, Universität Freiburg, Freiburg, Germany*
[23]*II. Physikalisches Institut, Georg-August-Universität Göttingen, Göttingen, Germany*
[24]*Institut für Physik, Universität Mainz, Mainz, Germany*
[25]*Ludwig-Maximilians-Universität München, München, Germany*
[26]*Fachbereich Physik, Bergische Universität Wuppertal, Wuppertal, Germany*
[27]*Panjab University, Chandigarh, India*
[28]*Delhi University, Delhi, India*
[29]*Tata Institute of Fundamental Research, Mumbai, India*
[30]*University College Dublin, Dublin, Ireland*
[31]*Korea Detector Laboratory, Korea University, Seoul, Korea*
[32]*CINVESTAV, Mexico City, Mexico*
[33]*Nikhef, Science Park, Amsterdam, the Netherlands*
[34]*Radboud University Nijmegen, Nijmegen, the Netherlands and Nikhef, Science Park, Amsterdam, the Netherlands*
[35]*Joint Institute for Nuclear Research, Dubna, Russia*
[36]*Institute for Theoretical and Experimental Physics, Moscow, Russia*
[37]*Moscow State University, Moscow, Russia*
[38]*Institute for High Energy Physics, Protvino, Russia*
[39]*Petersburg Nuclear Physics Institute, St. Petersburg, Russia*
[40]*Institució Catalana de Recerca i Estudis Avançats (ICREA) and Institut de Física d'Altes Energies (IFAE), Barcelona, Spain*
[41]*Stockholm University, Stockholm and Uppsala University, Uppsala, Sweden*
[42]*Lancaster University, Lancaster LA1 4YB, United Kingdom*
[43]*Imperial College London, London SW7 2AZ, United Kingdom*
[44]*The University of Manchester, Manchester M13 9PL, United Kingdom*
[45]*University of Arizona, Tucson, Arizona 85721, USA*
[46]*University of California Riverside, Riverside, California 92521, USA*
[47]*Florida State University, Tallahassee, Florida 32306, USA*
[48]*Fermi National Accelerator Laboratory, Batavia, Illinois 60510, USA*
[49]*University of Illinois at Chicago, Chicago, Illinois 60607, USA*
[50]*Northern Illinois University, DeKalb, Illinois 60115, USA*
[51]*Northwestern University, Evanston, Illinois 60208, USA*

[52]*Indiana University, Bloomington, Indiana 47405, USA*
[53]*Purdue University Calumet, Hammond, Indiana 46323, USA*
[54]*University of Notre Dame, Notre Dame, Indiana 46556, USA*
[55]*Iowa State University, Ames, Iowa 50011, USA*
[56]*University of Kansas, Lawrence, Kansas 66045, USA*
[57]*Kansas State University, Manhattan, Kansas 66506, USA*
[58]*Louisiana Tech University, Ruston, Louisiana 71272, USA*
[59]*Boston University, Boston, Massachusetts 02215, USA*
[60]*Northeastern University, Boston, Massachusetts 02115, USA*
[61]*University of Michigan, Ann Arbor, Michigan 48109, USA*
[62]*Michigan State University, East Lansing, Michigan 48824, USA*
[63]*University of Mississippi, University, Mississippi 38677, USA*
[64]*University of Nebraska, Lincoln, Nebraska 68588, USA*
[65]*Rutgers University, Piscataway, New Jersey 08855, USA*
[66]*Princeton University, Princeton, New Jersey 08544, USA*
[67]*State University of New York, Buffalo, New York 14260, USA*
[68]*Columbia University, New York, New York 10027, USA*
[69]*University of Rochester, Rochester, New York 14627, USA*
[70]*State University of New York, Stony Brook, New York 11794, USA*
[71]*Brookhaven National Laboratory, Upton, New York 11973, USA*
[72]*Langston University, Langston, Oklahoma 73050, USA*
[73]*University of Oklahoma, Norman, Oklahoma 73019, USA*
[74]*Oklahoma State University, Stillwater, Oklahoma 74078, USA*
[75]*Brown University, Providence, Rhode Island 02912, USA*
[76]*University of Texas, Arlington, Texas 76019, USA*
[77]*Southern Methodist University, Dallas, Texas 75275, USA*
[78]*Rice University, Houston, Texas 77005, USA*
[79]*University of Virginia, Charlottesville, Virginia 22901, USA*
[80]*University of Washington, Seattle, Washington 98195, USA*

We present a measurement of the ratio of top quark branching fractions $R = \mathcal{B}(t \to Wb)/\mathcal{B}(t \to Wq)$, where q can be a d, s, or b quark, in the lepton + jets and dilepton $t\bar{t}$ final states. The measurement uses data from 5.4 fb^{-1} of $p\bar{p}$ collisions collected with the D0 detector at the Fermilab Tevatron Collider. We measure $R = 0.90 \pm 0.04$, and we extract the Cabibbo-Kobayashi-Maskawa (CKM) matrix element $|V_{tb}|$ as $|V_{tb}| = 0.95 \pm 0.02$, assuming unitarity of the 3×3 CKM matrix.

The standard model (SM) of particle physics contains three generations of quarks. The top quark belongs to the third generation, and is of interest not only because of its large mass [1], but also because its decay has not been examined in great detail, and may prove to be inconsistent with the SM. The decay rate of the top quark into a W boson and a down-type quark q ($q = d\,s$, b) is proportional to $|V_{tq}|^2$, the squared element of the Cabibbo-Kobayashi-Maskawa (CKM) matrix [2]. Under the assumption of a unitary 3×3 CKM matrix, $|V_{tb}|$ is highly constrained to $|V_{tb}| = 0.999152^{+0.000030}_{-0.000045}$ [3], and the top quark decays almost exclusively to Wb. The existence of a fourth generation of quarks would remove this constraint and accommodate significantly smaller values of $|V_{tb}|$. A smaller value of $|V_{tb}|$ could be observed directly through the electroweak production of single top quarks, for which the cross section is proportional to $|V_{tb}|^2$, and could also affect the decay rates in the $t\bar{t}$ production channel. The latter can be used to extract the ratio of branching fractions R:

$$R = \frac{\mathcal{B}(t \to Wb)}{\mathcal{B}(t \to Wq)} = \frac{|V_{tb}|^2}{|V_{tb}|^2 + |V_{ts}|^2 + |V_{td}|^2}. \quad (1)$$

Given the constraints on the unitary 3×3 CKM matrix elements, R is expected to be $0.99830^{+0.00006}_{-0.00009}$. Along with a measurement of $|V_{tb}|$ using single top quark production, the measurement of R provides the possibility of a study of $|V_{tq}|$ [4].

This Letter presents a measurement of R using a data sample corresponding to an integrated luminosity of 5.4 fb^{-1} of $p\bar{p}$ collisions, collected with the D0 detector at the Fermilab Tevatron $p\bar{p}$ Collider at $\sqrt{s} = 1.96$ TeV. We present measurements in the lepton + jets (ℓ + jets) channel, in which one W boson from $t\bar{t} \to W^+qW^-\bar{q}$ production decays into a quark and an antiquark and the other into a charged lepton and a neutrino, and in dilepton ($\ell\ell$) final states, in which both W bosons decay into $\ell\nu$. We also present the combination of these two measurements. We consider events in which the charged leptons are either electrons or muons, produced directly from the W decay or

from the leptonic decay of a τ lepton. The result from the $\ell +$ jets channel corresponds to an improvement of the measurement using 0.9 fb^{-1} [5], in which we extracted $R > 0.79$ at a 95% CL. This is the first D0 measurement of R in the $\ell\ell$ channel. The CDF Collaboration has measured R in the $\ell +$ jets and $\ell\ell$ channels in 160 pb^{-1} of integrated luminosity [6], and found a limit of $R > 0.61$ at 95% CL.

Our measurement is performed by distinguishing between the standard decay mode of the top quark $t\bar{t} \to W^+ b W^- \bar{b}$ (indicated by bb), and decay modes that include light quarks ($q_l = d, s$): $t\bar{t} \to W^+ b W^- \bar{q}_l$ (bq_l) and $t\bar{t} \to W^+ q_l W^- \bar{q}_l$ ($q_l q_l$). The selection of an enriched $t\bar{t}$ sample and identification of jets from b quarks are crucial elements of the analysis.

The D0 detector [7] has a central tracking system consisting of a silicon microstrip tracker and a fiber tracker, both located within a 1.9 T superconducting solenoidal magnet, designed to optimize tracking at pseudorapidities $|\eta| < 3$ [8]. The liquid-argon and uranium calorimeter has a central section covering pseudorapidities $|\eta|$ up to ≈ 1.1, and two end calorimeters that extend coverage to $|\eta| \approx 4.2$ [9]. The outer muon system, covering $|\eta| < 2$, consists of a layer of tracking detectors and scintillation trigger counters in front of 1.8 T toroids, followed by two similar layers behind the toroids [10].

In the $\ell +$ jets channel, we rely on the event selections used for the measurement of the $t\bar{t}$ production cross section [11]. Details on object identification and selections are only briefly summarized as follows. We select $t\bar{t}$ events by taking advantage of their distinct topology. We require at least three jets within $|\eta| < 2.5$, with transverse momentum $p_T > 20$ GeV, of which at least one has to have $p_T > 40$ GeV. We require one electron (muon) of $p_T > 20$ GeV, $|\eta| < 1.1$ ($|\eta| < 2.0$) isolated from jets. In addition, events with a second isolated electron or muon of $p_T > 15$ GeV are removed in order to ensure that the $\ell +$ jets and $\ell\ell$ samples are statistically independent. The imbalance in transverse energy, $\not{E}_T$, must fulfill $\not{E}_T > 20$ GeV ($\not{E}_T > 25$ GeV) in the $e +$ jets ($\mu +$ jets) channel. The most important background in the $\ell +$ jets channel is from $W +$ jets events which can produce a similar final-state to $t\bar{t}$ events. There is also significant background contribution from multijet production, in which a jet is misidentified as an electron, or a muon from the semileptonic decay of a hadron appears isolated. Smaller background contributions arise from electroweak single top quark production, Drell-Yan and Z boson production (decaying to $l^+ l^- +$ jets) or diboson production (WW, WZ or ZZ). The multijet background is estimated from control samples in data [11], while the $t\bar{t}$ signal and electroweak backgrounds are simulated using Monte Carlo (MC) event generators ALPGEN and PYTHIA [12,13], and a GEANT-based [14] simulation of the D0 detector. Drell-Yan and Z boson production is normalized

to the next-to-next-to-leading order (NNLO) QCD prediction [15]. All other electroweak backgrounds are normalized to their next-to-leading order (NLO) cross sections, while the $W +$ jets background is normalized to data using an iterative procedure [11].

For the $\ell\ell$ channel, we use the same selections as used for the measurement of the $t\bar{t}$ cross section described in Ref. [16]. In this final state, the $t\bar{t}$ signature consists of two energetic, oppositely charged isolated leptons, large $\not{E}_T$ and two high p_T jets. We consider separately the three final states ee, $\mu\mu$ and $e\mu$. For the $e\mu$ final state, we also consider events with only one reconstructed jet. To select $t\bar{t}$ events, we require two isolated leptons, electrons or muons, with $p_T > 15$ GeV, $|\eta| < 1.1$ or $1.5 < |\eta| < 2.5$ ($|\eta| < 2$) for the electron (muon), and at least two jets with $p_T > 20$ GeV and $|\eta| < 2.5$. For $\mu\mu$ events we require $\not{E}_T > 40$ GeV. In the $e\mu$ channel, the sum of the transverse momenta of the lepton and two jets of highest p_T must be larger than 110 GeV. That sum must be higher than 105 GeV when only one jet is reconstructed. In the ee and $\mu\mu$ channels we use the $\not{E}_T$ significance to differentiate events with true $\not{E}_T$ from escaping neutrinos and events with $\not{E}_T$ arising from mismeasurement. The $\not{E}_T$ significance for each event is defined in terms of a likelihood discriminant constructed from the ratio of $\not{E}_T$ to its uncertainty [17]. The significance is required to correspond to more than five. The main background in the $\ell\ell$ final states is composed of Drell-Yan, Z boson production and diboson events, and is estimated using MC simulation, normalized to the NNLO and NLO cross sections, respectively. There is also a background from multijet events that we estimate from data [16].

We use a neural network (NN) b-tagging algorithm [18] to identify jets that contain b quarks, and thereby distinguish the bb, bq_l and $q_l q_l$ $t\bar{t}$ final states. The inputs to the NN include impact parameters of tracks associated with the jets, and the properties of secondary vertices within the jet. Only taggable jets, i.e., jets matched to a set of tracks, are considered by the NN. For each taggable jet, we obtain an output from the NN which ranges between zero and 12, with larger values more likely to correspond to jets originating from b quarks. Nontaggable jets are assigned the NN output value -1.

We pursue different strategies to measure R in the $\ell +$ jets and $\ell\ell$ channels. In the $\ell +$ jets channel, we count the number of jets that pass our threshold on the b-tagging NN output; this requirement has an efficiency for b jets of $55 \pm 4\%$, while admitting $1.5 \pm 0.1\%$ of light jets. The events are divided into subsamples according to lepton flavor (e or μ), the number of jets in the event (3 and >3), the data taking period (the first 1 fb^{-1} and the rest [11]), and the number of identified b jets (0, 1 or >1). The events are separated further using a multivariate kinematic discriminant in subsamples dominated by background, i.e., events with zero b-tagged jets, or one b-tagged jet in the sample

with exactly three jets, and zero b-tagged jets in the sample with more than three jets. This discriminant is based on a multivariate technique (random forest of decision trees [19]) and uses several variables that exploit the kinematic differences between $t\bar{t}$ signal and background. In addition to $t\bar{t}$ MC samples with SM decay $t\bar{t} \rightarrow WbWb$, samples for the decay modes including light quarks are generated with PYTHIA ($t\bar{t} \rightarrow WbWq_l$ and $t\bar{t} \rightarrow Wq_lWq_l$), for a top quark mass of $m_t = 172.5$ GeV. The expected number of $t\bar{t}$ events with m b-tagged jets can be written as

$$\mu_{t\bar{t}}^m(R, \sigma_{t\bar{t}}) = [R^2 \epsilon^m(bb) + 2R(1-R)\epsilon^m(bq_l)$$
$$+ (1-R)^2 \epsilon^m(q_lq_l)]\sigma_{t\bar{t}}\mathcal{B}^2(t \rightarrow Wq)L, \quad (2)$$

where ϵ^m is the product of the selection efficiency and the probability of an event to have m b-tagged jets for each of the three (bb, bq_l, and q_lq_l) decay modes, $\sigma_{t\bar{t}}$ is the $t\bar{t}$ production cross section and L is the integrated luminosity. A maximum likelihood fit is performed using the function

$$\mathcal{L}_{\ell+\text{jets}} = \prod_{i=1}^{N_{ch}} P[n^i, \mu^i(R, \sigma_{t\bar{t}}, \nu_k)]P[n^i_{MJ}, \mu^i_{MJ}]$$
$$\times \prod_k \mathcal{G}(\nu_k; 0, \text{SD}), \quad (3)$$

where i runs over the subsamples and bins of the multivariate discriminant, and $P[n, \mu(R, \sigma_{t\bar{t}}, \nu_k)]$ is the Poisson probability to observe n events for an expected number of $\mu(R, \sigma_{t\bar{t}}, \nu_k)$ events. The expectation $\mu(R, \sigma_{t\bar{t}}, \nu_k)$ is the sum of the expected number of $t\bar{t} \rightarrow bb$, bq_l and q_lq_l events and the expected number of background events. The observed and expected numbers of multijet events are denoted n^i_{MJ} and μ^i_{MJ}, and the Poisson terms $P[n^i_{MJ}, \mu^i_{MJ}]$ take into account the fluctuation of the number of multijet events within the statistical uncertainties with which it is determined in dedicated data samples. Figures 1(a) and 1(b) show the number of b-tagged jets in ℓ + jets events for data and simulation for $R = 0$, $R = 0.5$ and $R = 1$. To reduce the dependence of the measurement on the input $t\bar{t}$ cross section, we simultaneously extract $\sigma_{t\bar{t}}$ from data, taking

into account the three channels $t\bar{t} \rightarrow bb$, bq_l and q_lq_l. A parameter ν_k that accounts for each independent source of systematic uncertainty k is modeled by a Gaussian function $\mathcal{G}$ with a mean of zero and a width corresponding to one estimated standard deviation (SD) of that uncertainty. This procedure correlates systematic uncertainties among channels by using the same parameter for a common source of systematic uncertainty.

In the dilepton channels ee, $\mu\mu$, and $e\mu$ with at least 2 jets, we apply the NN b-tagging algorithm to the two jets of highest-p_T, and use the smaller of the two NN outputs to calculate the likelihood. as it yields the best expected precision on R for values close to unity. The b-tagging algorithm is applied to the single reconstructed jet in the $e\mu$ channel with exactly 1 jet. We construct the templates for the decay modes bb, bq_l, q_lq_l for $t\bar{t}$ as well as for all background components, forming the likelihood by running the product of Eq. (4) over all 14 bins of the NN discriminant in all four channels, yielding thereby a product with 56 factors:

$$\mathcal{L}_{\ell\ell} = \prod_{i=1}^{N_{ch}} P[n^i, \mu^i(R, \sigma_{t\bar{t}}, \nu_k)]\prod_k \mathcal{G}(\nu_k; 0, \text{SD}). \quad (4)$$

The expected number of events, $\mu_{t\bar{t}}^m(R, \sigma_{t\bar{t}}, \nu_k)$, is given by Eq. (2), where ϵ^m describes now the efficiency for the discriminant bin m, and ν_k can affect the individual components of $\mu_{t\bar{t}}^m(R, \sigma_{t\bar{t}})$. Figure 1(c) compares the distributions of the discriminant for predicted and observed events in the combined $\ell\ell$ final state.

Several systematic uncertainties can impact the measurement of R. We consider the same sources of systematic uncertainties as for the cross-section measurements in the ℓ + jets and $\ell\ell$ channels, and refer to Refs. [11,16] for details. The main source of systematic uncertainty on R is from the b-tagging probability. Other important contributions to the systematic uncertainty on R arise from the jet identification efficiency, jet energy scale and resolution, and uncertainties on the background normalization as well as on modeling of the signal. The latter includes
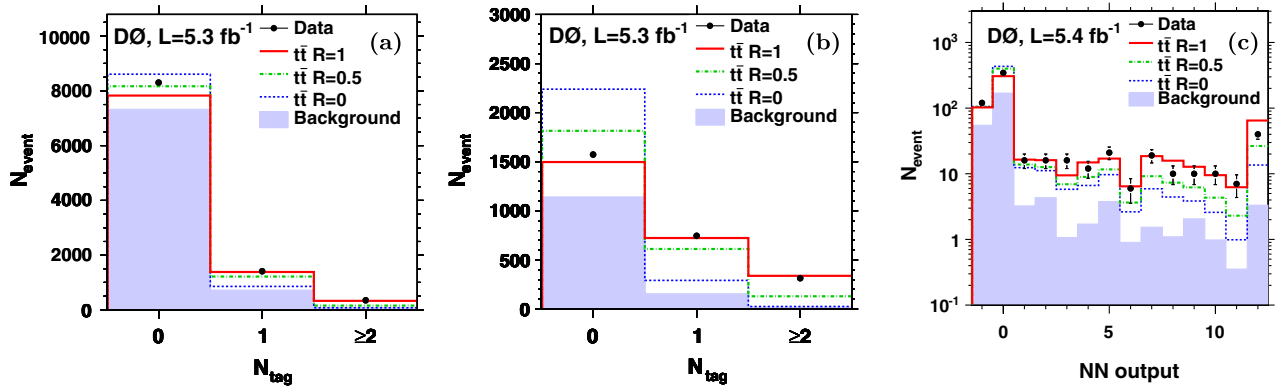

FIG. 1 (color online). (a) Number of b-tagged jets in ℓ + jets events with three jets and (b) at least four jets. (c) Distribution in the minimum b-tag NN output of the jets of highest p_T for dilepton final states.

contributions from higher-order effects, color reconnection, choice of parton distribution functions and initial and final-state gluon radiation. For consistency with Refs. [11,16] we also quote separately the smaller systematic contributions from limited number of events in the templates and the uncertainties on the heavy-flavor fraction for the W + jets process, the trigger efficiency and lepton identification. We account for the fact that uncertainties from jet identification, jet energy scale and resolution, b-jet identification, and higher-order corrections can affect the distribution of the discriminants in the ℓ + jets channel, and the NN discriminants in the $\ell\ell$ channel. We verify that the measurement of R does not depend on m_t by generating MC samples at different m_t values. In the ℓ + jets channel we obtain

$$R = 0.95 \pm 0.07(\text{stat} + \text{syst})$$

$$\sigma_{t\bar{t}} = 7.90^{+0.79}_{-0.67}(\text{stat} + \text{syst}) \text{ pb},$$

and in the $\ell\ell$ channel

$$R = 0.86 \pm 0.05(\text{stat} + \text{syst})$$

$$\sigma_{t\bar{t}} = 8.19^{+1.06}_{-0.92}(\text{stat} + \text{syst}) \text{ pb}.$$

The results are in agreement with each other, and the extracted cross sections are consistent with those from Refs. [11,16]. In these $\sigma_{t\bar{t}}$ measurements, we do not assume that $\mathcal{B}(t \to Wb) = 1$ as was done for the results in Refs. [11,16], but only require $\mathcal{B}(t \to Wq) = 1$. The combined measurement is obtained by fitting simultaneously all channels in the $\ell\ell$ and ℓ + jets final states. This yields

$$R = 0.90 \pm 0.04(\text{stat} + \text{syst})$$

$$\sigma_{t\bar{t}} = 7.74^{+0.67}_{-0.57}(\text{stat} + \text{syst}) \text{ pb}.$$

Table I summarizes the systematic uncertainties for the three results on R. The use of the complete distribution of the NN b-tagging algorithm in the dilepton channel allows us to reach a total uncertainty on the value of R similar to that obtained in the ℓ + jets channel despite the lower $t\bar{t}$ content of the dilepton sample. While in the $\ell\ell$ channel the statistical uncertainty still dominates, the ℓ + jets and the combined result are dominated by systematic uncertainties. If we assume unitarity of the CKM matrix, we extract $|V_{tb}| = 0.95 \pm 0.02$. Constraining the $t\bar{t}$ cross section to the SM value of $7.5^{+0.6}_{-0.7}$ pb [20] yields $R = 0.90 \pm 0.04$, identical within rounding errors to the result of the simultaneous fit.

Using the combined result, we extract intervals on R as well as on $|V_{tb}|$ from Eq. (1), assuming unitarity of the 3×3 CKM matrix. By applying the frequentist approach using the likelihood ratio ordering principle proposed by Feldman and Cousins [21], we obtain the intervals in R as 0.82–0.98 and V_{tb} as 0.90–0.99 at 95% CL. The expected limits are $R > 0.92$ and $V_{tb} > 0.96$ at 95% CL. Figure 2 shows the bands for 68%, 95%, and 99.7% confidence limits on R. Our result is compatible with the SM expectation at the 1.6% level. At 99.7% CL, we obtain $R > 0.77$ and $|V_{tb}| > 0.88$.

Without assumptions on the unitarity of the CKM matrix, we can write Eq. (1) as: $(1 - R)/R = (|V_{ts}|^2 + |V_{td}|^2)/|V_{tb}|^2$, and set a limit on this ratio at 99.7% CL of $(1 - R)/R < 0.30$.

To summarize, we have measured the ratio of branching fractions $R = \mathcal{B}(t \to Wb)/\mathcal{B}(t \to Wq)$ in both

TABLE I. Uncertainties on the measurements of R in the $\ell\ell$ and ℓ + jets channels as well as for the combination of the two. We evaluate the impact of each class of systematic uncertainties by calculating R and $\sigma_{t\bar{t}}$ using the corresponding parameters ν shifted by $\pm 1\text{SD}$ from their fitted mean. The final line shows the quadratic sum of the systematics, which can be slightly different from the one obtained with the global fit.

| Source	$\ell\ell$		ℓ + jets		Combination	
	+SD	−SD	+SD	−SD	+SD	−SD
Statistical	0.041	−0.042	0.030	−0.029	0.023	−0.023
Muon identification	0.002	−0.002	0.000	−0.001	0.001	−0.001
Electron identification and smearing	0.004	−0.004	0.000	−0.000	0.001	−0.002
Signal modeling	0.007	−0.006	0.009	−0.011	0.004	−0.006
Triggers	0.003	−0.003	0.001	−0.001	0.002	−0.002
Jet energy scale	0.008	−0.008	0.017	−0.016	0.003	−0.008
Jet reconstruction and identification	0.010	−0.009	0.018	−0.022	0.009	−0.013
b-tagging	0.018	−0.019	0.065	−0.056	0.034	−0.033
Background normalization	0.020	−0.020	0.004	−0.005	0.008	−0.010
W fractions matching + higher order effects	$\cdots$	$\cdots$	0.001	−0.001	0.001	−0.002
Instrumental background	0.013	−0.013	0.003	−0.004	0.005	−0.007
Luminosity	0.010	−0.010	0.001	−0.001	0.004	−0.004
Other	0.002	−0.002	0.000	−0.000	0.001	−0.001
Template statistics for template fits	0.002	−0.002	0.011	−0.011	0.010	−0.010
Quadratic sum of systematics	0.035	−0.035	0.071	−0.064	0.038	−0.040
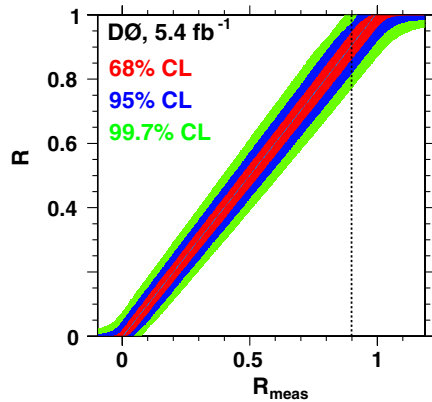
FIG. 2 (color online). Limit bands at 68%, 95%, and 99.7% CL on R, with the measured value (dotted line).

lepton + jets and dilepton channels. In the combined analysis, we find $R = 0.90 \pm 0.04$, which agrees within approximately 2.5 standard deviations with the SM prediction of R close to 1. This is the most precise determination of R to date. Using the approach of Ref. [21] and assuming the unitarity of the CKM matrix, we extract the interval at 95% CL on the element V_{tb} as 0.90–0.99.

---

*Deceased.

†With visitors from Augustana College, Sioux Falls, SD, USA.

‡With visitors from The University of Liverpool, Liverpool, United Kingdom.

§With visitors from SLAC, Menlo Park, CA, USA.

‖With visitors from University College London, London United Kingdom.

¶With visitors from Centro de Investigacion en Computacion-IPN, Mexico City, Mexico.

**With visitors from ECFM, Universidad Autonoma de Sinaloa, Culiacán, Mexico.

††With visitors from Universität Bern, Bern, Switzerland.

[1] The Tevatron Electroweak Working Group (CDF and D0 Collaborations), arXiv:1107.5255.

[2] N. Cabbibo, Phys. Rev. Lett. **10**, 531 (1963); M. Kobayashi and T. Maskawa, Prog. Theor. Phys. **49**, 652 (1973).

[3] K. Nakamura et al. (Particle Data Group), J. Phys. G **37**, 075021 (2010).

[4] J. Alwall et al., Eur. Phys. J. C **49**, 791 (2006).

[5] V. M. Abazov et al. (D0 Collaboration), Phys. Rev. Lett. **100**, 192003 (2008).

[6] T. Affolder et al. (CDF Collaboration), Phys. Rev. Lett. **95**, 102002 (2005).

[7] V. M. Abazov et al. (D0 Collaboration), Nucl. Instrum. Methods Phys. Res., Sect. A **565**, 463 (2006); M. Abolins et al., Nucl. Instrum. Methods Phys. Res., Sect. A **584**, 75 (2008); R. Angstadt et al., Nucl. Instrum. Methods Phys. Res., Sect. A **622**, 298 (2010);

[8] The pseudorapidity is defined as $\eta = -\ln[\tan(\theta/2)]$, where θ is the polar angle with respect to the proton beam.

[9] S. Abachi et al. (D0 Collaboration), Nucl. Instrum. Methods Phys. Res., Sect. A **338**, 185 (1994).

[10] V. M. Abazov et al. (D0 Collaboration), Nucl. Instrum. Methods Phys. Res., Sect. A **552**, 372 (2005).

[11] V. M. Abazov et al. (D0 Collaboration), Phys. Rev. D **84**, 012008 (2011).

[12] M. L. Mangano, M. Moretti, F. Piccinini, R. Pittau, and A. D. Polosa, J. High Energy Phys. 07 (2003) 001.

[13] T. Sjostrand, S. Mrenna, and P. Z. Skands, J. High Energy Phys. 05 (2006) 026.

[14] R. Brun and F. Carminati, CERN Program Library Long Writeup Report No. W5013, 1993 (unpublished).

[15] R. Gavin, Y. Li, F. Petriello, and S. Quackenbush, Comput. Phys. Commun. **182**, 2388, (2011).

[16] V. M. Abazov et al. (D0 Collaboration), arXiv:1105.5384 [Phys. Lett. B (to be published)].

[17] A. Schwartzman, Report No. FERMILAB-THESIS-2004-21.

[18] V. M. Abazov et al. (D0 Collaboration), Nucl. Instrum. Methods Phys. Res., Sect. A **620**, 490 (2010).

[19] A. Hoecker et al., Proc. Sci., ACAT (2007) 040.

[20] U. Langenfeld, S. Moch, and P. Uwer, Phys. Rev. D **80**, 054009 (2009).

[21] G. Feldman and R. Cousins, Phys. Rev. D **57**, 3873 (1998).